Geomechanics and Engineering, *Vol. 20, No. 2 (2020) 155-164*
DOI: https://doi.org/10.12989/gae.2020.20.2.155

Mechanical characteristics + differential settlement of CFG pile and cement-soil compacted pile about composite foundation under train load

Xuansheng Cheng*[1,2], Gongning Liu[1,2], Lijun Gong[1,2], Xinhai Zhou[2] and Baozhen Shi[3]

[1]*Key Laboratory of Disaster Prevention and Mitigation in Civil Engineering of Gansu Province, Lanzhou University of Technology, No. 287, Langongping Road, Qilihe District, Lanzhou, Gansu province, China*
[2]*Western Engineering Research Center of Disaster Mitigation in Civil Engineering of Ministry of Education, Lanzhou University of Technology, No. 287, Langongping Road, Qilihe District, Lanzhou, Gansu province, China*
[3]*China Railway 21st Bureau Group Sixth Engineering Co., LTD., No. 921, Beibinhe west road, Anning District, Lanzhou, Gansu province, China*

(Received February 15, 2019, Revised November 14, 2019, Accepted January 16, 2020)

Abstract. In recent years, the stability, safety and comfort of trains has received increased attention. The mechanical characteristics and differential settlement of the foundation are the main problems studied in high-speed railway research. The mechanical characteristics and differential settlement of the foundation are greatly affected by the ground treatment. Additionally, the effects of train load and earthquakes have a great impact. The dynamic action of the train will increase the vibration acceleration of the foundation and increase the cumulative deformation, and the earthquake action will affect the stability of the substructure. Earthquakes have an important practical significance for the dynamic analysis of the railway operation stage; therefore, considering the impact of earthquakes on the railway substructure stability has engineering significance. In this paper, finite element model of the CFG (Cement Fly-ash Gravel) pile + cement-soil compacted pile about composite foundation is established, and manual numerical incentive method is selected as the simulation principle. The mechanical characteristics and differential settlement of CFG pile + cement-soil compacted pile about composite foundation under train load are studied. The results show: under the train load, the neutral point of the side friction about CFG pile is located at nearly 7/8 of the pile length; the vertical dynamic stress-time history curves of the cement-soil compacted pile, CFG pile and soil between piles are all regular serrated shape, the vertical dynamic stress of CFG pile changes greatly, but the vertical dynamic stress of cement-soil compacted pile and soil between piles does not change much; the vertical displacement of CFG pile, cement-soil compacted pile and soil between piles change very little.

Keywords: composite foundation; train load; mechanical characteristics; differential settlement

1. Introduction

Based on the previous expression of train load, Pan and Pande (1984) proposed a function similar to the excitation form to express the vertical load of train. (Chua *et al.* 1995) modeled the complicated subway-soil-structure interaction problem by using the Finite Element Method (FEM), and an analytical model is incorporated to provide the train-loading input. Cheng *et al.* (2004) showed how to make numerical simulation of crushable soil by the discrete element method. Gupta *et al.* (2007) established two prediction models for calculating vibration from underground railways: the pipe-in-pipe model and the coupled periodic Finite Element–Boundary Element (FE–BE) model. Fang *et al.* (2018) proposed a coupling track-elastic subgrade bed-unsaturated subgrade model, and dynamic response of the unsaturated subgrade caused by moving train load was studied. Railway ballast particles undergo significant amount of breakage under repeated train load, Hossain *et al.* (2007) studied ballast breakage under cyclic loading. Siegel (2011) proposed a simplified model for a shallow foundation on composite ground. The proposed simplified model is applied using conventional geotechnical analyses for two hypothetical examples of shallow foundations undergoing compression settlement. Farhadian *et al.* (2012) analyzed the vibration of the tunnel under vehicle load. The concept of piled raft has been modified to new type of foundation named composite piled raft, and finite element method was applied to study the behaviour of this new type of foundation subjected to seismic forces (Sharma *et al.* 2015). Faro *et al.* (2015) conducted a series of lateral load pile tests on natural foundation and cemented soil. Li *et al.* (2016) studied the effect of dynamic cyclic loading and surcharge preloading method on the post-construction settlement of low embankments. Combined with the construction of Jinbao railway, Cui (2016) selected test sites, monitored and analyzed the settlement control effects of different engineering schemes, and proposed some basis for selecting reasonable foundation settlement calculation and analysis methods. The effective train load is utilized as an input to the structure-soil interaction problem to predict the ground vibrations and the environmental vibration levels of the structures (Lee *et al.* 2016). Based on the project in the loess area of Xi'an, and through the embedding of earth pressure box, Zhi *et al.* (2017) completed the static load test

*Corresponding author, Professor
E-mail: chengxuansheng@gmail.com

ISSN: 2005-307X (Print), 2092-6219 (Online)

of vertical reinforcement and single pile composite foundation. Cao and Qu (2017) used the high-speed railway foundation in seasonal frozen soil area as an example; through theoretical analysis, empirical methods, on-site observation, and finite element analysis, the ground temperature distribution law of foundation was analyzed. Sales *et al.* (2017) proposed a method to predict the load-settlement response of a pile group based on the response of a single pile. Cheng and Jing (2017) proposed two simplified methods to quantitatively treat the stability of composite foundation treated by a large number of compacted piles. Ismail (2018) proposed an empirical model based on product unit neural network to predict the load-deformation characteristics of pile-based support soil SPT values. On the basis of analyzing the relationship between pile-soil settlement and pile-soil, Liu *et al.* (2018) proposed the use of superimposed stress method to calculate the settlement of embankment with rigid-pile composite foundation. Lang *et al.* (2018) used the stress diffusion angle method to study the bearing capacity and settlement characteristics of prestressed thin-walled concrete pile composite foundation. Yin *et al.* (2018) tested the dynamic response of the pile-net composite subgrade under different vehicle speeds.

Combined with the existing literature and engineering cases, a study on the dynamic response of composite foundations is necessary, such as in frozen soil and saturated loess area. Due to the complex working principle of the composite foundation under the train load, the existing simulation principle includes the vehicle-orbit space coupling dynamic model, the simple train vertical vibration model and manual numerical incentive method; therefore, reasonable selection of an action principle can improve the accuracy of the finite element simulation.

2. The basic principle of train load and its finite element model

In this paper, combined with the design of a test section, the CFG pile + cement-soil compacted pile about composite foundation is selected to study its mechanical characteristics and differential settlement.

The strata of the test section are mainly Quaternary Upper Pleistocene alluvial sandy loess, fine gravel, sandstone and mudstone. The thickness of sandy loess is approximately 30.7 m - 50.9 m, the void ratio is about 1.0-1.1, which is high, and the bearing capacity is less than 180 kPa (Determined through local geological exploration data). The sandy loess belongs to the self-weight collapsible loess, and the collapsibility level is III. The thickness of wet soil layer is 10 m - 15 m, and the maximum freezing depth is 83 cm. Because of its complicated geological engineering conditions, the mechanical characteristics and differential settlement observation data of the high-speed railway composite foundation under train load are rarely given. Therefore, the CFG pile + cement-soil compacted pile about composite foundation is studied by a finite element method.

2.1 Basic principle of train load

2.1.1 Vehicle-orbit space coupling dynamics model

In the vehicle-orbit space coupling dynamics model, a nonlinear contact relationship is established between the wheel and rail based on the Hertz contact theory. The input track irregularity sample is used as the excitation, and a special calculation program is prepared to obtain the orbital force and the simple train vertical vibration model (Li, 2014).

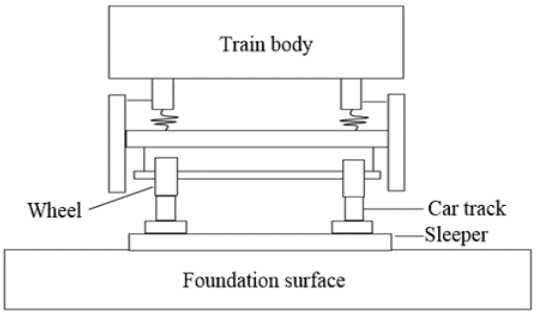

Fig. 1 Vehicle-orbit space coupling dynamics model

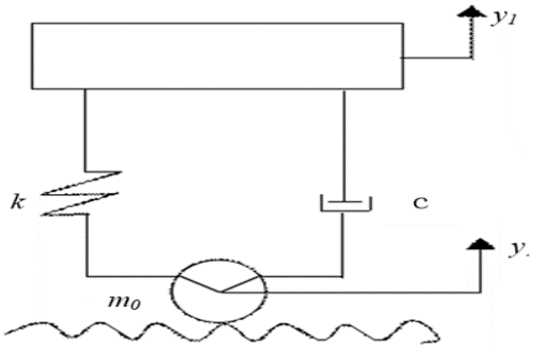

Fig. 2 Simple train vertical vibration model

2.1.2 Simple train vertical vibration model

The simplified train model is established considering only the vertical dynamic response of the train system to the track, assuming the train and the track are bound to each other, and ignoring the nonlinear factors in the system, including collisions and contacts (Fig. 1).

In Fig.2, k is the stiffness coefficient of spring; c is the damping coefficient buffer; y_1 is the absolute vertical displacement; m_0 is the train's unsprung mass. In the coordinate system shown in Fig. 2, the differential equation of the vertical analog train motion equilibrium is shown in Eq. (1).

$$m_2\left(\ddot{y}_1-\ddot{y}_0\right)+c\left(\dot{y}_1-\dot{y}_0\right)+k\left(y_1-y_0\right)=0 \tag{1}$$

Let $y_r=y_1-y_0$, then Eq. (2) is

$$m_2\ddot{y}_r+c\dot{y}_r+ky_r=0 \tag{2}$$

According to the D'Alembert's principle, the interaction force P(t) between the orbits is shown as Eq. (3),

$$\begin{aligned} P(t) &= (m_1+m_2)g+m_2\ddot{y}_1+m_2\ddot{y}_0 \\ &= (m_1+m_2)g+(m_1+m_2)\ddot{y}_0+m_2\ddot{y}_r \end{aligned} \tag{3}$$

There are two variables in the formula; however, the two variables are not independent. When the variables are

known, the solution of the wheel-rail contact force can be obtained using the above equation.

2.1.3 Manual numerical incentive method

According to the track irregularity requirements, a dynamic force function, including static load and a series of sinusoidal functions is used to simulate the train dynamic load (Li 2014), as shown in Eq. (4).

$$P_t = P_0 + P_1 \sin \omega_1 t + P_2 \sin \omega_2 t + P_3 \sin \omega_3 t \tag{4}$$

where P_0 indicates the static load of the wheel, and P_1, P_2, P_3 are a certain vibration load in the control standard.

If the unsprung mass of the train is M_0, the corresponding vibration load amplitude is shown in Eq. (5),

$$P_i = M_0 a_i \omega_i^2 \tag{5}$$

where a_i is a typical vector height in the I, II, III control standard, and ω_i is the circular frequency under the irregular vibration wavelength under the corresponding I, II, III control standards at the vehicle speed. The calculation formula of the circular frequency is Eq. (6), i.e.,

$$w_i = 2\pi v / L_i \tag{6}$$

where v is the running speed of the train, and L_i is the typical wavelength corresponding to the three control standards I, II, and III. This paper studies the simulation principle of the selected train by using manual numerical incentive method.

2.2 Constitutive model of soil

The deformation of soil consists of two stages: elastic deformation and plastic deformation. In numerical analysis of geotechnical engineering, the soil is modelled by elastoplastic model. The Mohr-Coulomb model is mainly suitable for granular materials under monotonic loading, so it is suitable for high speed railway foundation engineering.

2.2.1 Yield surface

The yield criterion of the Mohr-Coulomb model is the shear failure criterion. The shear yield surface function of the Mohr-Coulomb model is given by Eq. (7), i.e.,

$$F = R_{mc} q - p \tan \varphi - c = 0 \tag{7}$$

$R_{mc}(\Theta, \varphi)$ is calculated according to Eq. (8) as follows, and R_{mc} controls the shape of the yield surface in the π plane. φ is the inclination angle of the Mohr-Coulomb yield surface on the q-p stress surface, i.e., the internal friction angle，and $0° \leq \varphi \leq 90°$.

$$R_{mc} = \frac{1}{\sqrt{3}\cos\varphi} \sin\left[\Theta + \frac{\pi}{3}\right] + \frac{1}{3} cos\left[\Theta + \frac{\pi}{3}\right] \tan\varphi \tag{8}$$

where, c is the cohesion of the material; Θ is the polar angle, defined as $\cos(3\Theta) = \frac{r^3}{q^3}$, r is the third stress invariant.

The tensile damage criterion is based on Rankine, i.e.,

$$F_t = R_r(\Theta) q - p - \sigma_t = 0 \tag{9}$$

where, $R_r(\Theta) = \frac{2}{3}\cos(3\Theta)$, σ_t is tensile strength and it can vary with equivalent tensile plastic strain.

2.2.2 Plastic potential surface

The Mohr-Coulomb yield surface has sharp corners. If the associated flow law is used, the plastic flow direction is not unique at the sharp corners, which makes the convergence slow. ABAQUS uses the continuous smooth elliptic function as the plastic potential surface. The calculation is calculated according to Eq. (10), i.e.,

$$G = \sqrt{\left[(\varepsilon c_0 \tan\psi)^2 + (R_{mw} q)^2\right]} - p \tan\psi \tag{10}$$

where, ψ is the dilatancy angle; c_0 is the initial cohesion，that is, there is no cohesion when deformed; ε is eccentricity on the meridional plane. If ε=0, the plastic situation is a straight upward line, ABAQUS defaults it to be 0.1. Then $R_{mw}(\Theta, e, \varphi)$ control the shape of the plastic surface on the π surface, the value is calculated according to Eq. (11), i.e.,

$$\frac{4\left(1-e^2\right)\cos^2\Theta + (2e-1)^2}{2\left(1-e^2\right)\cos\Theta + (2e-1)\sqrt{\left[4\left(1-e^2\right)(\cos\Theta)^2 + 5e^2 - 4e\right]}}, \quad R_{mw}\left(\frac{\pi}{3}, \varphi\right) = R_{mw} \tag{11}$$

where, e is the eccentricity of the surface, mainly controls the shape of the $\Theta=0 \sim \frac{\pi}{3}$ plastic surface on the π surface. The default value is calculated according to Eq. (12), i.e.,

$$e = \frac{3 - \sin\varphi}{3 + \sin\varphi} \tag{12}$$

The e calculated according to the above formula ensures that the plastic potential surface is tangent to the yield π surface at the corners where the surface is subjected to tension and compression. Of course, the reader can also specify the size of e, but the scope must be: $0.5 < e \leq 1.0$.

2.2.3 Hardening law

The hardening or softening of the shear plastic surface in ABAQUS is achieved by controlling the magnitude of the cohesion c, and the relationship between c and the equivalent plastic strain must be specified during use. The equivalent strain is calculated according to Eq. (13):

$$\overline{\varepsilon} = \sqrt{\left(\frac{2}{3} e_{ij} e_{ij}\right)} \tag{13}$$

where, e_{ij} is partial strain tensor. This paper combines the linear elastic model and the Mohr-Coulomb model to simulate CFG pile + cement-soil compacted pile composite foundation.

2.3 Finite element model of the CFG pile + cement-soil compacted pile composite foundation

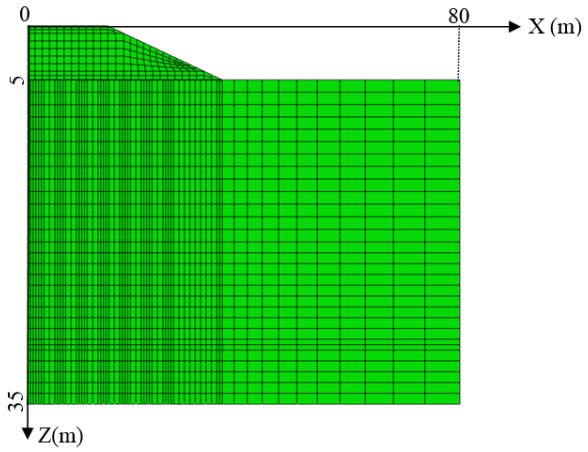

Fig. 3 CFG pile + cement-soil compacted pile composite foundation model

The model of CFG pile + cement-soil compacted pile composite foundation is established by using FEM (Fig. 3).

2.3.1 Boundary conditions and material contacts

In the complex model of composite foundation, in order to calculate quickly, in the first analysis step, the distribution type Geostatic is first changed to Static general, and the accurate maximum displacement change amount is obtained through trial calculation, and then the distribution type is changed to Geostatic to calculate. In the initial analysis step, the displacement in the x, y, and z directions of the bottom of the foundation soil is restricted, and the left and right sides displacement of the x direction are restricted, and the displacements in the y direction are restricted to the front and rear sides.

In the model, the tangential contact between the pile side and the foundation soil is frictional contact; the contact characteristics between the pile side and the soil body: the normal behavior is hard contact. Tangential behavior characteristics: the friction formula uses the penalty function, the friction coefficient u=tanφ. The bottom of the pile is bound to the bottom of the foundation hole. The normal contact between the bottom of the pile and the bottom of the foundation hole is a hard contact, and only the normal force is transmitted, so the friction coefficient is taken as 0. The contact between the top of the pile and the bottom of the cushion is a hard contact, where in the top of the pile is the main contact surface, and the bottom of the cushion is the appurtenant contact surface, and the friction coefficient is taken as 0.

2.3.2 Layers contact

The contact problem is a typical nonlinear problem. Not only is the mechanical model of the contact surface itself nonlinear, but also the contact is a special discontinuous condition, which is not easy to converge in numerical calculation. The ABAQUS mechanical model mainly defines the normal behavior and the Tangential Behavior model of the contact surface.

Normal behavior model: The normal behavioral model of the contact surface is also known as the Pressure-Overclosure Model, which includes hard contact and soft contact. Hard contact means that the two soils transmit normal pressure when pressed, the pressure is not restricted, and the normal pressure is not transmitted when there is a gap between the two objects; this behavior limits the possible penetration and penetration. However, when the contact condition is from the "on" state (the gap is positive) to the “closed” state (the gap is zero), the contact pressure has undergone a large change, and sometimes the contact calculation is difficult to converge. The essence of soft contact is to slow the rate of change between contact pressure and interference when closing.

Tangential behavioral model: The tangential behavior of the contact surface is usually simulated by frictional behavior. When the contact surface is in a closed state (normal contact pressure), the contact surface can transmit tangential stress, that is, the friction. When the frictional force is less than the limit value τ_{crit}, the contact surface is in a bonded state; when the frictional force is greater than the limit value, the contact surface begins to undergo relative slip deformation, that is, in a slip state. In this paper, the Coulomb Friction Theory is used in the CFG pile + cement-soil compacted pile about composite foundation model, and the frictional coefficient u is used to express the frictional characteristics between the contact surfaces.

① Ultimate shear stress

The ultimate shear stress is calculated according to Eq. (14), i.e.,

$$\tau_{\text{crit}} = uP \tag{14}$$

where, P is the normal contact pressure.

② Elastic slip deformation

Under ideal conditions, the contact surface has no shear deformation before the slip state, and at this time, the numerical calculation is difficult. Therefore, ABAQUS introduces “elastic slip deformation”, that is, a small amount of relative slip is allowed when the main and the slave surfaces are bonded together. The top of pile is the main layer while the bottom of the cushion is the slave layer. Determine the elastic slip deformation according to the length of the unit on the contact surface, and use the penalty stiffness algorithm to calculate.

2.3.3 Possible water table

In this paper, it is assumed that there is no ground water in the model, that is, we don’t consider the effect of water table.

2.3.4 Geometry of composite foundation model

Calculated width: In order to understand the settlement and deformation law of the foundation, the 3D model of CFG pile + cement-soil compacted pile composite foundation is established and finite element analysis is carried out. The bottom of the composite ground is 32m wide, and the calculated width of the foundation soil is taken as 2.5 times the composite foundation bottom width, so the entire foundation width of the model in this paper is 80 m.

Calculated depth: Considering the additional stress of the pile and the influence depth of the settlement deformation and calculating it, the calculated depth of the

Table 1 Geometry of composite foundation model (m)

Foundation treatment	Calculated width	Calculated depth	Calculated length	Embankment height
CFG pile + cement soil compacted pile composite foundation	80	30	4	5

Table 2 The calculation parameters of CFG pile + cement-soil compacted pile about composite foundation model

Name	Density (kg/m³)	Elastic Modulus (Pa)	Poisson's ratio	Internal friction angle /°	Constitutive model
Subgrade bed surface	2000	1×10^7	0. 23	30	Mohr-Coulomb
Subgrade bed bottom	1950	8×10^7	0. 26	32	Mohr-Coulomb
Cushion	2000	2×10^8	0. 3	-	Elasticity
CFG pile	2500	2.55×10^{10}	0. 17	-	Elasticity
Cement-soil compacted pile	2000	1×10^8	0. 23	-	Elasticity
Sandy loess	1900	2×10^7	0. 3	25	Mohr-Coulomb
Fine gravel	2200	0	0. 28	35	Mohr-Coulomb
Mudstone	2435	5×10^{10}	0. 30	34	Mohr-Coulomb
Sandstone	2530	7×10^{10}	0. 25	35	Mohr-Coulomb
Name	Dilatancy angle (°)	Cohesion (Pa)	Lateral pressure coefficient	Thickness (m)	Constitutive model
Subgrade bed surface	0	2×10^4	-	0. 7	Mohr-Coulomb
Subgrade bed bottom	0	3×10^4	-	3. 5	Mohr-Coulomb
Cushion	-	-	-	0. 8	Elasticity
CFG pile	-	-	0. 2	15	Elasticity
Cement-soil compacted pile	-	-	0. 2	8	Elasticity
Sandy loess	0	3.5×10^4	0. 5	20	Mohr-Coulomb
Fine gravel	-	0	0. 5	4	Mohr-Coulomb
Mudstone	-	5×10^4	0. 5	1	Mohr-Coulomb
Sandstone	-	9×10^4	0. 5	5	Mohr-Coulomb

Table 3 Track and train uniform load

Track form	Track load and train load				Interline load q_2 (kN/m²)
	Distribution width b (m)	Track load q_1 (kN/m²)	Train load q_2 (kN/m²)	Total load q (kN/m²)	
CRTSI	3. 0	12. 6	41. 7	54. 3	13. 2
CRTSII	3. 25(2. 95)	11. 6(14. 3)	38. 5(42. 4)	50. 1(56. 7)	14. 1(12. 0)
CRTSIII	3. 1	13. 7	40. 4	54. 1	2. 3
CRTSI	3. 4	13. 7	36. 8	50. 5	1 1
Orbital track	3. 4	17. 3	36. 8	54. 1	10. 7

foundation soil is calculated as twice the length of the longest pile, and the largest pile's length of the CFG pile + cement soil compacted pile composite foundation is 15 m, so the calculated depth of the composite foundation is 30 m.

Calculated length: Because the foundation extends symmetrically on both sides along the line direction, the length in this direction is twice the pile spacing, and the spacing between CFG piles is designed to be 2 m. The geometric dimensions of the composite foundation model are shown in Table 1.

2.3.5 The parameters of the model

The calculation parameters of CFG pile + cement-soil compacted pile composite foundation model are found in Table 2**.**

2.3.6 Dynamic boundary conditions and mechanical damping

The damping coefficient of the boundary normal direction is calculated by $\rho c_p \sum_i^{i=1} A_i$; the linear elastic stiffness coefficient is calculated by $4G/R\sum_i^{i=1} A_i$; and the boundary tangential damping coefficient is calculated by $\rho c_s \sum_i^{i=1} A_i$ .The linear elastic stiffness coefficient is calculated by $2G/R\sum_i^{i=1} A_i$. Among them, $\sum_i^{i=1} A_i$ is the unit area around the node on the artificial boundary surface. G is the dielectric modulus ρ is the medium density. R is the distance from the embankment to the boundary surface. c_p is the medium compression wave velocity. c_s is the dielectric shear wave velocity (Sobhan *et al.* 2012).

2.3.7 Train load calculation

On the track line of the CFG pile + cement-soil compacted pile composite foundation embankment, the load amplitude curve with the time interval of 4 s is selected. According to 6.1.15 of *Code for Design of High Speed Railway* (Ministry of Railways of the People's Republic of China 2014), the uniform load of track and train is shown in Table 3.

3. Mechanical characteristics under train load

To observe the vertical dynamic displacement of the pile top of the CFG pile + cement-soil compacted pile composite foundation under train load, select the following test section observations: at section 0.000 m plane, observation points of CFG pile (observation point 1, observation point 4, observation point 5, observation point 6), cement-soil compacted pile (observation point 2) and soil between the piles (observation point 3) are shown in Fig. 4.

3.1 Vertical dynamic stress

3.1.1 CFG pile vertical dynamic stress

Under the train load, by extracting the vertical dynamic stress of observation point 1 from the CFG pile of the composite ground at 0.000 m plane and selecting the peak for dynamic stress-time history analysis, the time-history

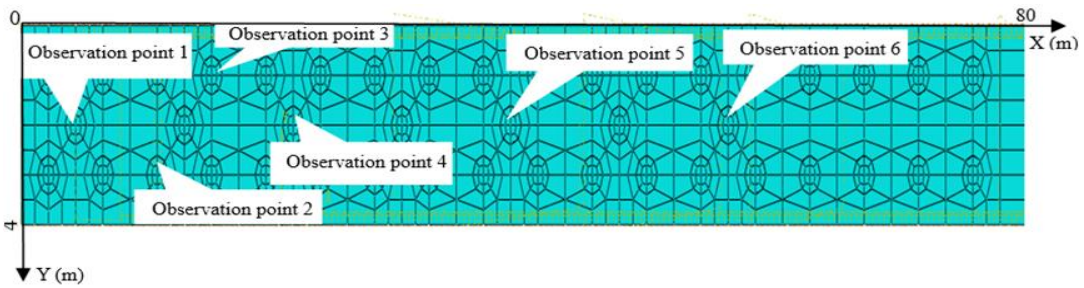

Fig. 4 Plane layout of the observation points about composite foundation at the section 0. 000 m plane

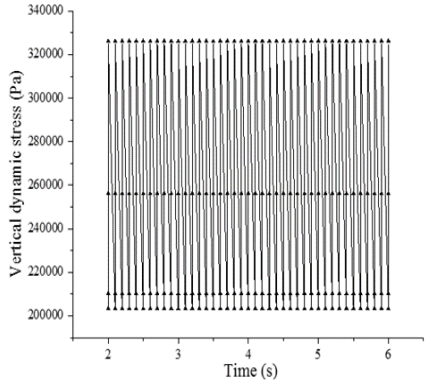

Fig. 5 Vertical dynamic stress-time history curve of CFG pile at observation point 1

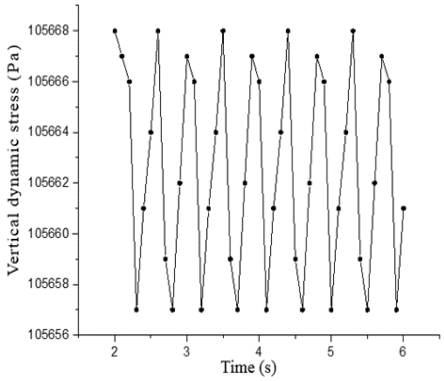

Fig. 6 Vertical dynamic stress-time history curve of the cement-soil compacted pile observation point 2

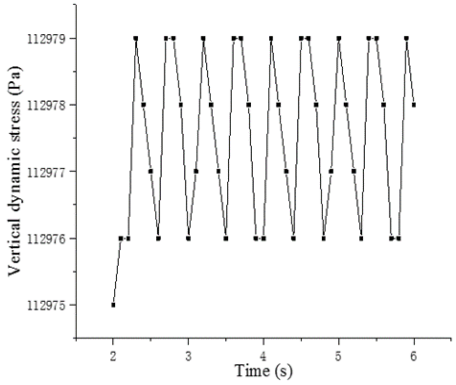

Fig. 7 Vertical dynamic stress-time history curve of the observation point 3 about soil between piles

curve of the vertical dynamic stress of observation point 1 about CFG pile is shown in Fig. 5.

Fig. 5 shows that the time-history curve of the vertical dynamic about the CFG pile is a regular "zigzag"; therefore, the vertical dynamic stress is increased at any time. For example, at the time of 3.1 s, the first vertical dynamic stress value of the CFG pile is 203256 Pa, the second vertical dynamic stress value of the CFG pile is 256090 Pa, the third vertical dynamic stress value of the CFG pile is 210151 Pa, the fourth vertical dynamic stress value of the CFG pile is 326094 Pa, and the maximum peak and the minimum peak are different by 122838 Pa. Therefore, under the train load, the vertical dynamic stress of the CFG pile observation point 1 in the 0.000 m plane changes greatly.

3.1.2 Vertical dynamic stress of cement-soil compacted pile

Under the train load, by extracting the vertical dynamic stress of the cement-soil compacted pile with the composite foundation 0.000 m plane and selecting the peak dynamic stress-time history analysis, the vertical dynamic stress-time history curve of the cement-soil compacted pile observation point 2 is obtained (Fig. 6).

Fig. 6 shows that the time-history curve of the vertical dynamic stress about the cement-soil compacted pile is a regular "zigzag shape". There are three peaks within 0.5 s (from the time of 3 s to the time of 3.5 s). The vertical peak value of the first peak point (time 3 s) is 105667 Pa, the vertical value of the second peak point (time 3.25 s) is 105657 Pa, vertical dynamic stress value at the third peak point (time 3.5 s) is 105668 Pa, and the maximum peak and the minimum peak are 11 Pa apart. Therefore, under the train load, the vertical dynamic stress of the cement-soil compacted piles at the 0.000 m plane observation point 2 is not very large.

3.1.3 Vertical dynamic stress of the soil between piles

Under the train load, the vertical dynamic stress of the soil observation point between the 0.000 m plane piles on the composite foundation is extracted, and the dynamic stress-time history analysis is carried out to select the peak. The vertical dynamic stress-time history curve of the observation point 3 about soil between piles is shown in Fig. 7.

Fig. 7 shows that the time-history curve of the vertical dynamic stress between the cement-soil compacted piles is a regular "zigzag". There are five peaks in the 1.5 s between the time of 3 s and the time of 4.5 s. The vertical peak value of the first peak point (at the time of 3.25 s) is 112979 Pa and the second peak point (at the time of 3.5 s) has a

vertical dynamic stress value of 112976 Pa; the maximum peak and the minimum peak are 3 Pa apart. Therefore, under the train load, the vertical dynamic stress of the soil between piles about observation point 3 is not very large at the 0.000 m plane.

3.2 Side friction

Under the train load, the side frictional resistance curve of CFG pile along the pile depth is shown in Fig. 8.

Fig. 8 shows that under the train load, the lateral frictional resistance of the CFG pile in the composite foundation of CFG pile + cement-soil compacted pile reaches a maximum value of -50000 Pa from the top of the pile to 11 m of the pile, and the side frictional resistance decreases to 0 at 13 m of the pile. Therefore, 13 m is the neutral point. From 13 m of the CFG pile to the bottom section of the pile, the positive frictional resistance reaches maximum value at 14 m of the pile body. Additionally, the trend of observation point 1, observation point 4, observation point 5 and observation point 6 changes consistently.

3.3 Soil arching effect

Under the train load, the vertical stress is taken from the CFG pile + cement-soil compacted pile composite foundation with 0.5 m and 1.0 m sections in the Y direction, and the respective contour diagrams are drawn, as shown in Figs. 9-10.

Fig. 9 shows that under the train load, the vertical stress equivalent characteristics of the cement-soil compacted pile at the 0.5 m section are obvious, especially within the 1 m height range from the top of the embankment to the shoulder of the cement-soil compacted pile. Here, an equivalence line of the stress appears. Therefore, a cylindrical soil arch with the same size as the pile diameter is formed between the two piles. From the embankment to the cement-soil compacted pile, the soil arching effect is weakened, and only the vertical stress at the edge between the two piles is equivalent, forming a semicircular soil arch with a diameter of 0.6 m. Due to the self-weight of the embankment, the self-weight of the pile and the downward transfer of the train load, the equivalence line of the stress also appears in the 1 m range between the two piles at the bottom of the cement-soil compacted pile. Therefore, a cylindrical soil arch of the same size as the diameter of the pile is formed between the two piles.

Fig. 10 shows that under the train load, the vertical stress equivalent characteristics of the 2 m at the top of the CFG pile in the 1.0 m section is obvious, especially in the 1 m range from the top of the CFG pile to the shoulder of the road. Here, the vertical stress shows an isoline, but no vertical stress isoline appears between the two CFG piles. The reason for this analysis is that the CFG pile is stronger than the cushion layer; the top of the CFG pile penetrates into the cushion layer, and the vertical stress between the CFG piles shows the contour from the embankment to the cement-soil compacted pile due to the decrease of train load and foundation weight. Furthermore, the CFG pile top penetration is small, and the equivalent vertical stress range

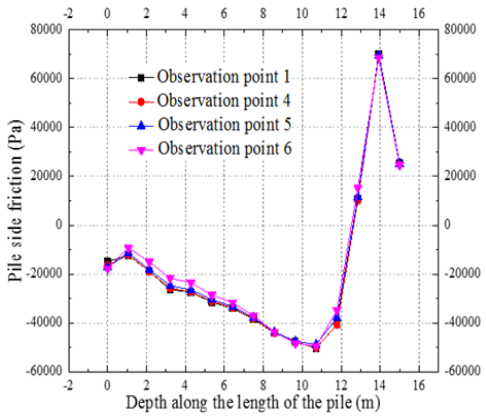

Fig. 8 Side friction resistance curve of the CFG pile along pile length

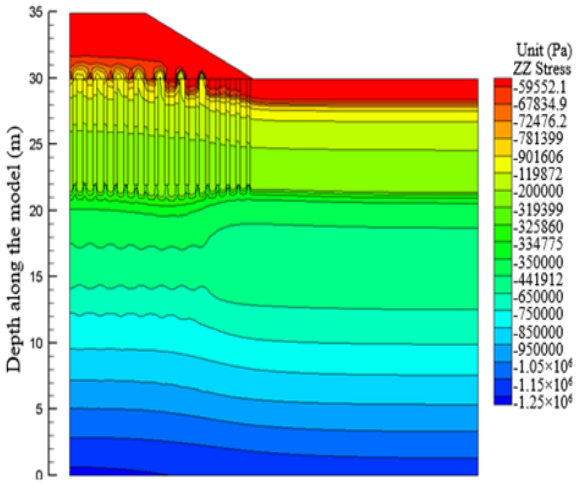

Fig. 9 Vertical stress cloud diagram of the cement-soil compacted pile at the 0. 5m section

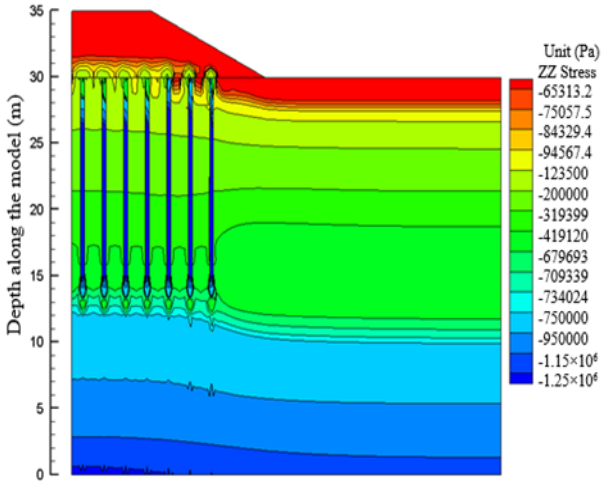

Fig. 10 Vertical stress cloud diagram of the CFG pile at the 1. 0 m section

of the pile is reduced. Due to the weight of the embankment, the weight of the pile or the downward transfer of the train load, the CFG pile transmits its upper stress to the lower soil layer, and a stress isoline appears within 1.25 m of the bottom end of the pile.

4. Settlement characteristics under train load

Under the train load, the vertical dynamic displacement of the CFG pile observation point about the composite ground 0.000 m plane and the observation point of the cement-soil compacted pile are extracted, and the vertical displacement of the CFG pile observation point, the cement-soil compacted pile observation point, and the inter-pile soil observation point are selected to conduct a vertical displacement-time history analysis.

4.1 CFG pile settlement characteristics

Under the train load, the displacement cloud diagram of the CFG pile + cement-soil compacted pile composite foundation is shown in Fig.11. The CFG pile displacement-time history curve is shown in Fig. 12.

Fig. 12 shows that the vertical displacement-time history curve of the CFG pile is a regular "zigzag", and there are three peaks in 0.5 s between the time of 3 s and the time of 3.5 s. The first peak point (time 3 s) is vertical and has a displacement value of 8.8693 mm, the second peak point (time 3.25 s) has a vertical displacement value of 8.8699 mm, the third peak point (time 3.5 s) has a vertical displacement value of 8.8693 mm, and the maximum peak value differs from the minimum peak value by 0.0006 mm. Therefore, under the train load, the vertical displacement of the 0.000 m plane CFG pile observation point 1 is not very large.

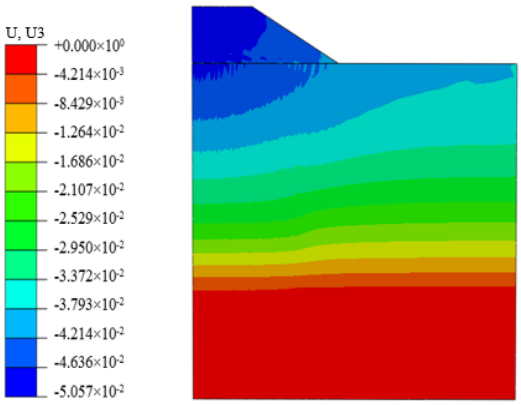

Fig. 11 Vertical displacement cloud diagram of composite foundation (mm)

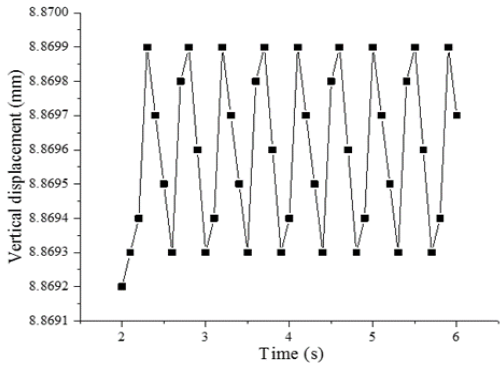

Fig. 12 Vertical displacement-time history curve of the CFG pile

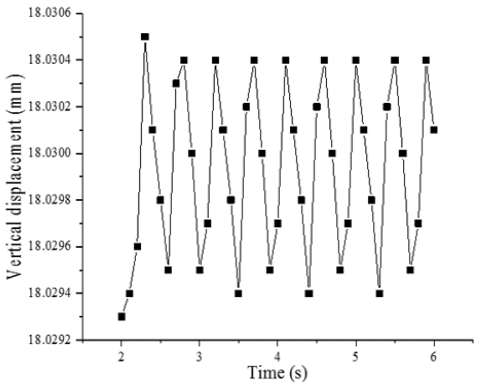

Fig. 13 Displacement-time history curve of the cement-soil compacted pile

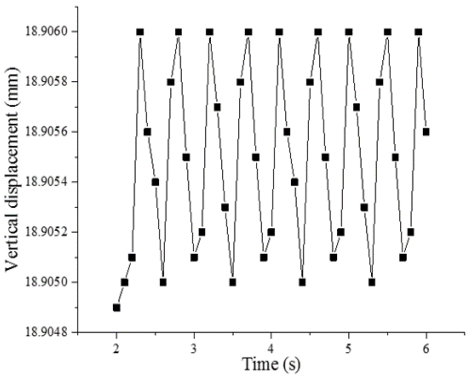

Fig. 14 Displacement-time history curve of the soil between piles

4.2 Settlement characteristics of cement-soil compacted piles and soil between piles

Under the train load, the displacement-time history curves for the observation point 2 of cement-soil compacted pile, and the displacement-time history curves for the observation point 3 of soil between piles are shown in Fig. 13 and Fig. 14, respectively.

Fig. 13 shows that the vertical displacement-time history curve of the cement-soil compacted pile is a regular “zigzag shape”, and five peaks appear in 1s between the time of 4 s and the time of 5 s. The vertical displacement value of the first peak point (time 4 s) is 18.0295 mm. At second peak point (time 4.25 s), the vertical displacement value is 18.0304 mm, and the third peak point (time 4.5 s) has a vertical displacement value of 18.0294 mm. The difference between the maximum peak value and the minimum peak value is approximately 0.001 mm. Therefore, under the train load, the vertical displacement of the cement-soil compacted pile of the 0.000 m plane observation point 2 change little.

Fig. 14 shows that the time-history curve of the soil between the piles vertical displacement is a regular “zigzag shape”, and five peaks appear within 1 s (from the time 4 s to the time 5 s). At the first peak point (time 4 s), the vertical displacement value is 18.9051 mm. At the second peak point (time 4.25 s), the vertical displacement value is 18.9060 mm. At the third peak point (time 4.5 s), the vertical displacement value is 18.9050 mm. The maximum

peak value and the minimum peak value are 0.001 mm apart. Therefore, under the train load, the vertical displacement of the soil measuring point 3 between the 0.000 m plane piles is not very large, and it is consistent with the vertical displacement of the cement-soil compacted pile.

5. Conclusions

• The advantages and disadvantages of the three simulation principles commonly used under train load are analyzed. The manual numerical incentive method is used to determine the finite element simulation principle of the test section; the model size, dynamic load parameters, and time load amplitude parameters of the CFG pile + cement-soil compacted pile composite foundation train are determined.

• The load amplitude of the 4 s is input at the middle point of the left rail of the line centerline. The CFG pile, cement-soil compacted pile and the vertical dynamic stress-time history curve of the soil in the 0.000 m plane are all regular "zigzag". Therefore, the vertical dynamic stress of the CFG pile changes greatly. The changes in the vertical dynamic stress of cement-soil compacted piles and soil between piles are very little, and the neutral point of the body friction of the CFG pile is located at about 7/8 the pile length (from the top of pile to the bottom of pile). Neutral point is the important turning point of the pile's side friction resistance (from negative to positive). This neutral point of pile body can make a reference for designers and constructors of this field. Furthermore, a cylindrical soil arch is formed between the cement-soil compacted piles, and the effective height of the soil arch is 1 time the pile spacing. Therefore, cylindrical soil arches are not formed between the CFG piles, and the vertical stress is equivalent to only 1 m in the top and bottom ends of the CFG pile.

• Under the train load, the vertical displacement-time history curves of CFG piles, cement-soil compacted piles and soil between piles are all regular "zigzag", which shows that the vertical displacement of CFG piles, cement-soil compacted piles and soil between piles change little, that is, the settlement of CFG pile + cement-soil compacted pile composite foundation is small under train load.

Acknowledgments

This paper is a part of the National Natural Science Foundation of China (Grant number: 51968045 and 51478212), and a part of science and technology project in China Railway 12th Bureau Group Co. LTD. (Grant number: 14B-3), and a part of science and technology project in China Railway Construction Investment Group Co. LTD. (Grant number: 17-C21).

References

Cao, Y.M. and Qu, J.T. (2017), "Influence of subgrade differential settlement on riding performance of high-speed train", *Proceedings of the International Congress and Exhibition Sustainable Civil Infrastructures: Innovative Infrastructure Geotechnology*, Egypt, July.

Cheng, X.S. and Jing, W. (2017), "Calculation models and stability of composite foundation treated with compacted piles", *Geomech. Eng.*, **13**(6), 929-946. https://doi.org/10.12989/gae.2017.13.6.929.

Cheng, Y.P., Bolton, M.D. and Nakata, Y. (2004), "Crushing and plastic deformation of soils simulated using DEM", *Geotechnique*, **54**(2), 131-141. https://doi.org/10.1680/geot.2004.54.2.131.

Chua, K.H., Lo, K.W. and Balendra, T. (1995), "Building response due to subway train traffic", *J. Geotech. Eng.*, **121**(11), 747-754. https://doi.org/10.1061/(ASCE)0733-9410(1995)121:11(747).

Cui, W.X. (2016), "Research on the settlement characteristics of subgrade in the test section of Tianjin-Baoding railway", *J. Railway Eng. Soc.*, **33**(10), 38-89. https://doi.org/10.3969/j.issn.1006-2106.2016.10.008.

Fang, R., Lu, Z., Yao, H.L., Luo, X.W. and Yang, M.L. (2018), "Study on dynamic responses of unsaturated railway subgrade subjected to moving train load", *Soil Dyn. Earthq. Eng.*, **115**, 319-323. https://doi.org/10.1016/j.soildyn.2018.08.037.

Farhadian, H., Aalianvari, A. and Katibeh, H. (2012), "Optimization of analytical equations of groundwater seepage into tunnels: A case study of Amirkabir tunnel", *J. Geol. Soc. India*, **80**, 96-100. https://doi.org/10.1007/s12594-012-0122-z.

Faro, V.P., Consoli, N.C., Schnaid, F., Thome A. and Lopes, L.S. (2015), "Field tests on laterally loaded rigid piles in cement treated soils", *J. Geotech. Geoenviron. Eng.*, **141**(6), 06015003(1-7). https://doi.org/ 10.1061/(ASCE)GT.1943-5606.0001296.

Gupta, S., Hussein, M.F.M., Degrande, G., Hunt, H.E.M. and Clouteau, D. (2007), "A comparison of two numerical models for the prediction of vibrations from underground railway traffic", *Soil Dyn. Earthq. Eng.*, **27**(7), 608-624. https://doi.org/10.1016/j.soildyn.2006.12.007.

Hossain, Z., Indraratna, B., Darve, F. and Thakur P. K. (2007), "DEM analysis of angular ballast breakage under cyclic loading", *Geomech. Geoeng.*, **2**(3), 175-181. https://doi.org/10.1080/17486020701474962.

Ismail, A. (2018), "ANN-based empirical modelling of pile behaviour under static compressive loading", *Front. Struct. Civ. Eng.*, **12**(4), 594-608. https://doi.org/10.1007/s11709-017-0446-2.

Lang, R.Q., Yan S.W., Sun L.Q., Ji, Y.C. and Chen, J. (2018), "Analysis of stress diffusion angle method for PTC pile composite foundation", *Eur. J. Environ. Civ. Eng.*, **22**, 434-448. https://doi.org/10.1080/19648189.2017.1369462.

Lee, J.H., Lee J.J., Choi, J.S. and Yun, C.B. (2016), "A semi-analytical approach to predict ground vibration by identification of soil properties and train-transit loads", *Adv. Struct. Eng.*, **15**(6), 1013-1029. https://doi.org/10.1260/1369-4332.15.6.1013.

Li, G.Q. (2014), "The dynamic characteristics of CFG pile composite foundation research under the high-speed train load and fatigue life prediction of CFG pile", Master thesis, Xi'an University of Architecture and Technology, Xi'an, China

Li, G.W., Nguyen, T.N. and Amenuvor, A.C. (2016), "Settlement prediction of surcharge preloaded low embankment on soft ground subjected to cyclic loading", *Mar. Georesour. Geotechnol.*, **34**(2), 154-161. https://doi.org/10.1080/1064119X.2014.985860.

Liu, J.F., Zheng, G. and Gong, X.N. (2018), "Superimposed stress method to calculate settlement of embankment with rigid-pile composite foundation", *Chin. J. Geotech. Eng.*, **40**(11),1995-2002. https://doi.org/10.11779/CJGE201811005.

Ministry of Railways of the People's Republic of China (2014),

"TB10621-2014 Code for design of high speed railway", Ministry of Railways of the People's Republic of China, Beijing, China.

Pan, C.S. and Pande, G.N. (1984), "Preliminary deterministic finite element study on a tunnel driven in loess subjected to train loading", *China Civ. Eng. J.*, **17**(4), 18-28. https://doi.org/10.15951/j.tmgcxb.1984.04.002.

Sales, M.M., Prezzi, M., Salgado, R., Choi, Y.S. and Lee, J. (2017), "Load-settlement behaviour of model pile groups in sand under vertical load", *J. Civ. Eng. Manage.*, **23**(8) ,1148-1163. https://doi.org/10.3846/13923730.2017.1396559.

Sharma, V. J., Vasanvala, S.A. and Solanki, C.H. (2015), "Study of cushioned composite piled raft foundation behaviour under seismic forces", *Australian J. Civ. Eng.*, **13**(1), 32-39. https://doi.org/10.1080/14488353.2015.1092636.

Siegel, T.C. (2011), "Simplified settlement model for a shallow foundation on composite ground with rigid piles", *DFI J. J. Deep Found. Inst.*, **5**(1), 68-72. https://doi.org/10.1179/dfi.2011.006.

Sobhan, K., Ramirez, J. and Reddy, D. (2012), "Cement stabilization of highly organic subgrade soils to control secondary compression settlement", *Transport. Res. Rec. J. Transport. Res. Board*, **2310**, 103-112. https://doi.org/10.3141/2310-11.

Yin F., Liu H.L., Chen Y.M., Li J.B. and Zhou, H. (2018), "Dynamic response of XCC pile-geogrid composite foundation of expressways influenced by vehicles with different speeds", *Chin. J. Geotech. Eng.*, **40**(3), 546-553. https://doi.org/10.11779/CJGE201803020.

Zhi, B., Li, G., Wang Y.X., Guo, J. and Wang, F. (2017), "Experimental research on load-bearing property of CFG pile composite foundation", *Build. Struct.*, **47**(23), 100-102. https://doi.org/10.19701/j.jzjg.2017.23.020.

CC